Original Article
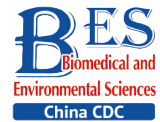
Numerical Simulation on Radon Retardation Behavior of Covering Floats in Radon-Containing Water[*]

LIU Shu Yuan[1], ZHANG Li[2], YE Yong Jun[3], and DING Ku Ke[1,2,#]

1. National Institute for Radiological Protection, Chinese Center for Disease Control and Prevention, Beijing 100088, China; 2. Office for Public Health Management, Chinese Center for Disease Control and Prevention, Beijing 102206, China; 3. Key Discipline Laboratory for National Defense for Biotechnology in Uranium Mining and Hydrometallurgy, University of South China, Hengyang 421001, Hunan, China

Abstract

Objective   This study aimed to efficiently reduce the release of radon from water bodies to protect the environment.

Methods   Based on the sizes of the experimental setup and modular float, computational fluid dynamics (CFD) was used to assess the impact of the area coverage rate, immersion depth, diffusion coefficient, and radon transfer velocity at the gas–liquid interface on radon migration and exhalation of radon-containing water. Based on the numerical simulation results, an estimation model for the radon retardation rate was constructed. The effectiveness of the CFD simulation was evaluated by comparing the experimental and simulated variation values of the radon retardation rate with the coverage area rates.

Results   The effect of radon transfer velocity on radon retardation in water bodies was minor and insignificant according to the appropriate value; therefore, an estimation model of the radon retardation rate of the coverage of a radon-containing water body was constructed using the synergistic impacts of three factors: area coverage rate, immersion depth, and diffusion coefficient. The deviation between the experimental and simulated results was < 4.3%.

Conclusion   Based on the numerical simulation conditions, an estimation model of the radon retardation rate of covering floats in water bodies under the synergistic effect of multiple factors was obtained, which provides a reference for designing covering floats for radon retardation in radon-containing water.

Key words: Radon-containing water; Radon retardation rate; CFD; Coverage experiment; Optimized design

INTRODUCTION

Radon (^{222}Rn) is a radioactive inert gas produced by the decay of Ra (^{226}Ra). Relevant studies have shown a significant correlation between radon exposure and increased incidence of leukemia and lung cancer[1,2]. After smoking, radon is the second most common cause of human lung cancer[3]. The United Nations Scientific Committee on the Effects of Atomic Radiation

(UNSCEAR) pointed out that radon is soluble in water, and its solubility decreases rapidly with an increase in temperature[4]. ^{222}Rn in water is a potentially important source of health hazards to human beings because the rocks and soils through which the water circulation process flows, as well as the water itself, contain the nuclide ^{226}Ra.

The presence of uranium minerals in a region leads to a radon concentration in groundwater between 1.13 and 457.35 Bq·L^{-1}. Approximately 10% of the radon concentration in the study sample is higher than the maximum contamination level of 100 Bq·L^{-1} recommended by the World Health Organization (WHO)[5]. The bottom sediment carried by the river basin into which wastewater from uranium mining facilities is discharged has relatively high natural radioactivity, and the radon concentration dissolved in the water is also relatively high. The radium content in the bottom sediment ranges from 100 to 2,000 Bq·kg^{-1}, and the sludge from mine water treatment has a radium content as high as 1,690 Bq·kg^{-1}[6]. This shows that radon-containing water bodies in uranium mines pose a radioactive pollution hazard to the surrounding environment that cannot be ignored, which endangers the health of uranium mine workers and simultaneously restricts a sustainable social and economic development.

Reducing radon exhalation from the surface of radon-containing water bodies has become a key problem that urgently needs to be addressed for environmental treatment. Current research has focused on the bioremediation of radon-containing water bodies[7-9], establishing multiple barriers to them[10], setting up closed chambers in the upper parts of ponds[5] and using nanomaterials to absorb radon[11]. However, most nanomaterials cannot be synthesized on a large scale at low cost, which limits their practical application in radionuclide contamination management. The use of isolated and confined spaces is also ineffective. Because of the change in the air exchange rate and water level, the radon in the air layer in the confined room is released into the outside atmosphere, and the radon concentration in the air around the mine increases, leading to an increase in the radon dose to the staff and the surrounding public.

In radon pollution prevention and control, the cover method has become one of the effective methods to retard the exhalation of airborne radon[12-14]. Ye et al. designed and manufactured modular floats and studied the effectiveness of modular surface-covering floats in retarding radon

release from water surfaces[15]. Their study shows that the proposed modular floats are effective in retarding radon release. Therefore, a numerical simulation was conducted to optimize the coverage effect by considering economic and environmental factors. Numerical simulations are significant in experimental research and practical applications. Experiments to determine the effects of the area coverage rate, diffusion coefficient, and radon transfer velocity on the radon retardation rate have proven to be expensive and costly. A simulation can better reveal the law of the experimental response and be more systematic. Furthermore, the experimental period is longer, and the simulation is more efficient. In addition, the consistency between the simulation and experimental results suggests that the simulation can provide guidance for future engineering design optimization. In terms of research methods, computational fluid dynamics (CFD) has been better applied in the migration and exhalation of airborne radon[16-18]. In view of this, this study considers radon-containing water bodies (including the bottom mud of water bodies) in uranium mines as the research object and adopts a method combining physical experiments and numerical simulations. It establishes a migration model of radon-containing water bodies under different physical parameters based on the water body radon release simulation experimental device and the actual size of the modular float. Further, it compares the numerical simulation results of the radon-retardation effect of radon-containing water bodies with the experimental results. This research has significant scientific value for enriching and developing the theory and methods of radon protection for water bodies in uranium mines. It optimizes the design of radon protection by covering water bodies, thus protecting the environment around mines as well as the health of workers and the public.

METHODS

Physical Model

As shown in Figure 1, based on the size of the designed modular floats and the experimental setup constructed by Ye et al.[15], a three-dimensional model was established to study the radon retardation law for covering floats in radon-containing water bodies. The model is primarily composed of two parts: (1) a sediment-containing water body, with the overlying water layer

representing the pure water zone and the sediment layer representing the porous zone. The length (a_1) of the water body is 0.485 m, the width (b_1) is 0.335 m, the thickness of the overlying water (h_w) is 0.1 m, and the sediment thickness (h_s) is 0.03 m. (2) Some combined modular floats with side length (a_2) of the single modular float of 0.155 m and thickness (b_2) of 0.045 m.

Numerical Method

Geometric Model As one of the geometric model pairs, the uncovered and float-covered (with area coverage rate of 29.6%) geometric models are shown in Figure 2. The length × width × thickness of the uncovered water body is 0.485 m × 0.335 m × 0.130 m, whereas the length × width × thickness of the float-covered area is 0.310 m × 0.155 m × 0.040 m (two combined floats)[15].

Mathematical Model The diffusion migration equation of radon in the overlying water layer under steady-state conditions is

$$D_w\left[\frac{\partial^2 C_w}{\partial x^2} + \frac{\partial^2 C_w}{\partial y^2} + \frac{\partial^2 C_w}{\partial z^2}\right] - \lambda C_w + \alpha_w = 0 \quad (1)$$

where C_w is water radon concentration in the overlying water layer (x, y, z); Bq/m^3; D_w is the radon diffusion coefficient in the water, m^2·s^{-1}; λ is the radon decay constant, 2.1×10^{-6} s^{-1}; and α_w is the free radon production rate for the overlying water layer, Bq·m^{-3}·s^{-1}.

The steady-state radon diffusion migration equation for a radium-containing sediment layer is as follows:

$$D_{w,s}\left[\frac{\partial^2 C_{w,s}}{\partial x^2} + \frac{\partial^2 C_{w,s}}{\partial y^2} + \frac{\partial^2 C_{w,s}}{\partial z^2}\right] - \lambda C_{w,s} + \frac{\eta\alpha_w + (1-\eta)\,\alpha_s}{\eta} = 0 \quad (2)$$

where $C_{w,s}$ is the water radon concentration in the sediment layer (x,y,z), Bq·m^{-3}; $D_{w,s}$ is the radon diffusion coefficient in the sediment layer, m^2·s^{-1}; and $\alpha_{w,s}$ is the free radon production rate for the sediment, Bq·m^{-2}·s^{-1}.

α_w and $\alpha_{w,s}$, as well as $D_{w,s}$ are given in Equation (1) and Equation (2), as follows:

$$\alpha_w = \lambda A_w \quad (3)$$

$$\alpha_{w,s} = \lambda\rho_s A_{w,s} S_e \quad (4)$$
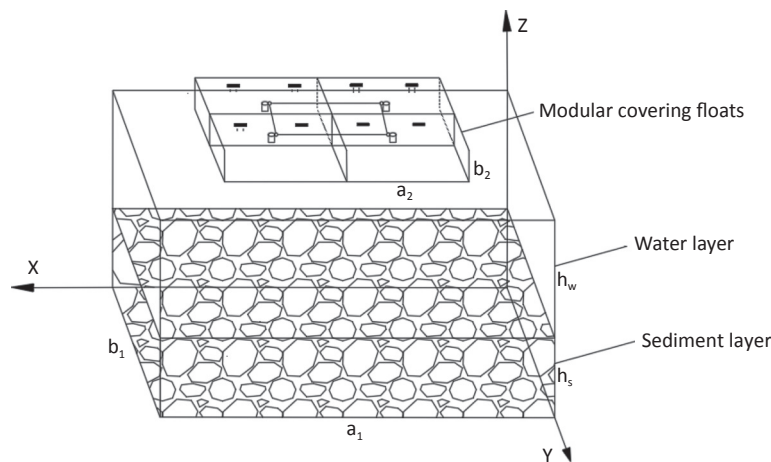

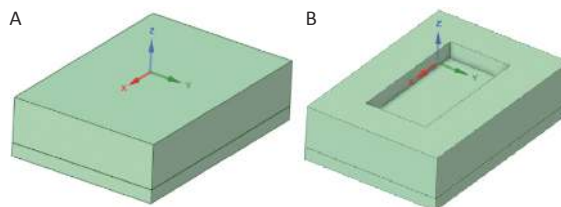**Figure 1.** Three-dimensional diagram of water with modular floats.

Figure 2. Geometric model of water body (A) uncovered and (B) float-covered (with area coverage rate of 29.6% and immersion depth of 0.04 m) geometric models.

$$D_{w,s} = \tau D_w \qquad (5)$$

where A_w is the radium activity concentration in the overlying water layer; Bq·m^{-3}; $A_{w,s}$ is the radium activity concentration in the sediment, Bq·kg^{-1}; ρ_s is the density of the sediment, kg·m^{-3}; S_e is the radon emanation coefficient of the sediment, %; and τ is the dimensionless pore distortion of the sediment layer, which is taken as 0.66[19].

The radon retardation rate f can be expressed as follows:

$$f = \left(1 - \frac{JS}{J_0 S_0}\right) \times 100\% \qquad (6)$$

where J_0 is the average radon exhalation rate of the exposed water without coverage, Bq·m^{-2}·s^{-1}; S_0 is the exposed surface area of the water body without coverage, m^2; J is the average radon exhalation rate of the exposed water with coverage, Bq·m^{-2}·s^{-1}; and S is the exposed surface area of water with coverage, m^2.

The radon release rate of the water surface can be calculated as

$$R_{w,s} = \frac{\bar{J}_w S_f}{\alpha_{w,s} V_s + \alpha_w V_w} \qquad (7)$$

where $\bar{J}_w$ is the average radon exhalation rate of the water surface, Bq·m^{-2}·s^{-1}; S_f is the exposed surface area of the water body, m^2; V_s is the volume of the sediment layer, m^3; and V_w is the volume of the overlying water layer, m^3.

Boundary Conditions The bottom and four walls of the water body are set as wall boundaries ($\frac{\partial C}{\partial Z} = 0$). A user-defined function (UDF) is established based on the relationship between the radon transport flux at the gas–liquid interface and the radon exhalation rate of the overlying water surface, that is, $k(C_{w1} - \beta C_a) = -D_{w1}\frac{\partial C_{w1}}{\partial Z}$. When the radon concentration in the air is 0 Bq·m^{-3}, the boundary condition of the water surface is $C_{w1} = \frac{-D_{w1}\frac{\partial C_{w1}}{\partial Z}}{k}$. When the radon concentration in the air is C_a Bq·m^{-3}, the boundary condition of the water surface is $C_w = \frac{-D_{w1}\frac{\partial C_{w1}}{\partial Z} + k\beta C_a}{k}$. In this study, the radon concentration in the air was considered to be 0 Bq·m^{-3}.

Meshing Division Using the laminar flow model and COUPLE algorithm, a UDF was written to set the radium activity concentration and the radon diffusion coefficient in the overlying water and sediment layers. The criterion for numerical convergence was that the maximum relative difference between two successive iterations should be less than 10^{-11}.

The geometric model was meshed using a hexahedral-structured mesh to simulate the migration and exhalation laws of radon in water under different coverage conditions and to save computation time under a limited configuration. An independent test of the geometric model mesh was performed to ensure the accuracy and reliability of the simulation results. Three different mesh sizes were set in the water body when the area coverage rate was 29.6% and the immersion depth was 0.04 m: 0.002, 0.003, and 0.004 m, and the number of meshes were 2,362,480, 712,494, 295,482, respectively. The results of the radon exhalation rate on the water surface were 0.037,930,82, 0.037,911,93, and 0.037, 876,45 Bq·m^{-2}·s^{-1}. The relative deviation of the calculation results for the different meshes can be ignored; therefore, a size of 0.003 m was selected for meshing. The number of cells with which all cases were calculated ranged from 223,000 to 712,494.

Simulation Parameters In light of the pertinent literature, the radium activity concentration (A_w) in the overlying water layer ranged from 1 to 30 Bq·L^{-1}[20] and that in sediment (A_s) ranged from 0.15 to 13.7 Bq·g^{-1}[21-23]. As a result of biological disturbance and environmental temperature, the equivalent diffusion coefficient (D_w) of radon in the overlying water layer ranged from 2 × 10^{-9} to 2.19 × 10^{-5} m^2·s^{-1}[24-26], whereas the radon transfer velocity at the gas–liquid interface (k), without or at low wind speed, was between 1 × 10^{-7} and 1 × 10^{-5} m·s^{-1}[27-30]. Accordingly, A_w was taken as 20 Bq·L^{-1}, and A_s was assumed as 5.25 Bq·g^{-1}. To simulate the different unperturbed states in the water body, D_w was taken as 1.0 × 10^{-9}, 5 × 10^{-9}, 1.0 × 10^{-8}, and 5 × 10^{-8} m^2·s^{-1}, and K was assumed as 1 × 10^{-7}, 5 × 10^{-7}, 1 × 10^{-6}, and 5 × 10^{-6} m·s^{-1} respectively.

Coverage Parameters In addition to the above values of physical parameters, the area coverage rate (P) was taken as 29.6%, 59.1%, and 88.7% and the immersion depth (h) was assumed as 0.02, 0.04, 0.06, and 0.08 m, respectively, owing to the difference in coverage conditions[15].

Experimental Verification

Experimental Setup and Related Parameters

Figure 3[15] shows the experimental setup, which was primarily composed of two parts: (1) a sample holding setup (an acrylic container with an inner length of 0.485 m and an inner width of 0.335 m); (2) a radon concentration measurement system consisting of a RAD7 radon detector (Durridge Company Inc., USA), a gas drying unit, and vinyl tubing; and 3) some combined modular floats covering the water surface.

Estimation Method of Radon Diffusion Coefficient

The estimation model for the radon diffusion coefficient in water was established, as shown in Figure 4.

The radon diffusion migration equation of water body is

$$D_w \frac{\partial^2 C_w}{\partial Z} - \lambda C_w + a_w = 0 \qquad (8)$$

The boundary conditions are as follows:

$$J_{w2} = D_w \frac{\partial C}{\partial Z}\Big|_{z=0} \qquad (9)$$
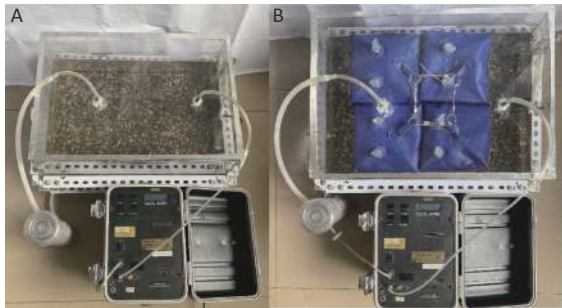
$$C(Z=0) = C_{w1} \qquad (10)$$

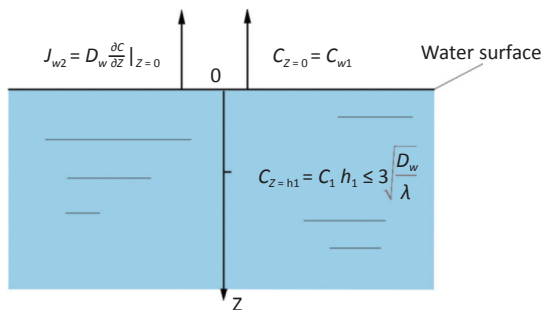**Figure 3.** Experimental setup:[15] (A) uncovered water, (B) covered water.

Figure 4. Estimation model diagram of radon diffusion coefficient in water.

where C_{w1} is the surface radon concentration in the pure water zone, Bq·m^{-3}.

The analytical solution of radon concentration in Equation (10) is

$$C(Z) = \frac{a_w}{\lambda}\left[1 - \cosh_w\left(Z\sqrt{\frac{\lambda}{D_w}}\right)\right] + \left(\frac{J_{w2}}{\sqrt{\lambda D_w}}\sinh_w Z\sqrt{\frac{\lambda}{D_w}}\right) + C_{w1}\cosh_w\left(Z\sqrt{\frac{\lambda}{D_w}}\right)$$

$$(11)$$

where h_w is the depth of water, m.

Based on these following parameters: $C_{z=0\,m}$ = 181,427 ± 4,540 Bq·m^{-3}, $C_{z=0.02\,m}$ = 348,276 ± 6,500 Bq·m^{-3}, $\bar{J}_{w2}$ = 0.127 ± 0.001 Bq·m^{-2}·s^{-1}, α_w = 0.0134 Bq·m^{-3}·s^{-1}, and λ = 2.1 × 10^{-6} s^{-1}, the radon diffusion coefficient in water (D_w = (1.58 ± 0.041) × 10^{-8} m^2·s^{-1}) was obtained by solving Equation (11).

Comparison of Experimental and Simulated Results

Figure 5 shows the experimental and simulated variation values of the radon retardation rate with the area coverage rate at an immersion depth of 0.04 m. The figure shows the simulated values for two diffusion coefficients (D_w = 1 × 10^{-9} m^2·s^{-1} and D_w = 1 × 10^{-8} m^2·s^{-1}) as well as the measured values for two types of water bodies (unperturbed and perturbed water bodies). It can be observed from Figure 5 that when the immersion depth is the same, the numerical simulation results of the variation trend of the radon retardation rate in radon-containing water with the area coverage rate match well with the experimental results; that is, both
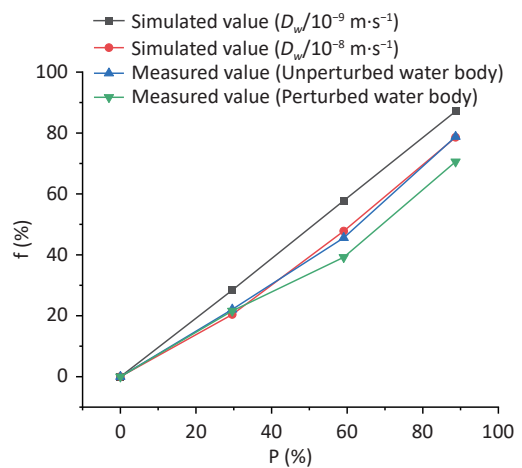

Figure 5. Variation of radon retardation rate with area coverage rate at immersion depth of 0.04 m. D_w, radon diffusion coefficient.

increase with an increase in the area coverage rate. Particularly, a high match between the simulated variation values ($D_w = 1 \times 10^{-8}$ m$^2 \cdot$s^{-1}) results and the experimental variation values ($D_w = (1.58 \pm 0.041) \times 10^{-8}$ m$^2 \cdot$s^{-1}) is observed. Therefore, it is feasible to use CFD to study the radon retardation behavior of covering floats in radon-containing water.

RESULTS

Effect of Parameters on Radon Concentration

The distribution of radon concentrations in the water bodies with different coverage rates is shown in Figure 6A. The following can be observed from Figure 6A: 1) the concentration around the float is high in the center and low in the periphery, showing a gradient distribution around the float. 2) The radon concentration distribution in water under different coverage rates is affected by the diffusion coefficient. When the diffusion coefficient (D_w) is less than 1×10^{-9} m$^2 \cdot$s^{-1}, the radon concentration distribution does not change significantly with the increase in area coverage rate; when the diffusion coefficient (D_w) is greater than 1×10^{-8} m$^2 \cdot$s^{-1}, the larger the area coverage rate is, the larger the concentration gradient in the sediment layer, and the concentration gradient around the float becomes smaller. 3) Under the same diffusion

coefficient, the average radon concentration of the water body progressively increases with an increase in the area coverage rate. For example, when the diffusion coefficient is 1×10^{-8} m$^2 \cdot$s^{-1} and the area average rate increases from 29.6% to 88.7%, the average radon concentration in the overlying water layer increases from 239,556.9 to 325,718.7 Bq$\cdot$m^{-3}, whereas that in the sediment layer increases from 2,296,108 to 2,305,312 Bq$\cdot$m^{-3}.

The radon concentration distributions in water bodies at different immersion depths are shown in Figure 6B. It can be observed from Figure 6B: 1) under the same diffusion coefficient, the radon concentration gradient in the area around the float and in the sediment area increases with increasing immersion depth. 2) Regardless of how the diffusion coefficient changes, the radon concentration in both the overlying water and sediment layers increases with the increase in immersion depth. For example, when the diffusion coefficient is 1×10^{-8} m$^2 \cdot$s^{-1} and the immersion depth varies from 0.02 to 0.08 m, the average radon concentration in the overlying water layer increases from 281,541.9 to 320,034.7 Bq$\cdot$m^{-3} and that in the sediment layer increases from 839,690.5 to 960,979.8 Bq$\cdot$m^{-3}.

Radon concentration distributions in water bodies with different diffusion coefficients are exhibited in Figure 6C, which shows that under the same coverage conditions, the radon concentration
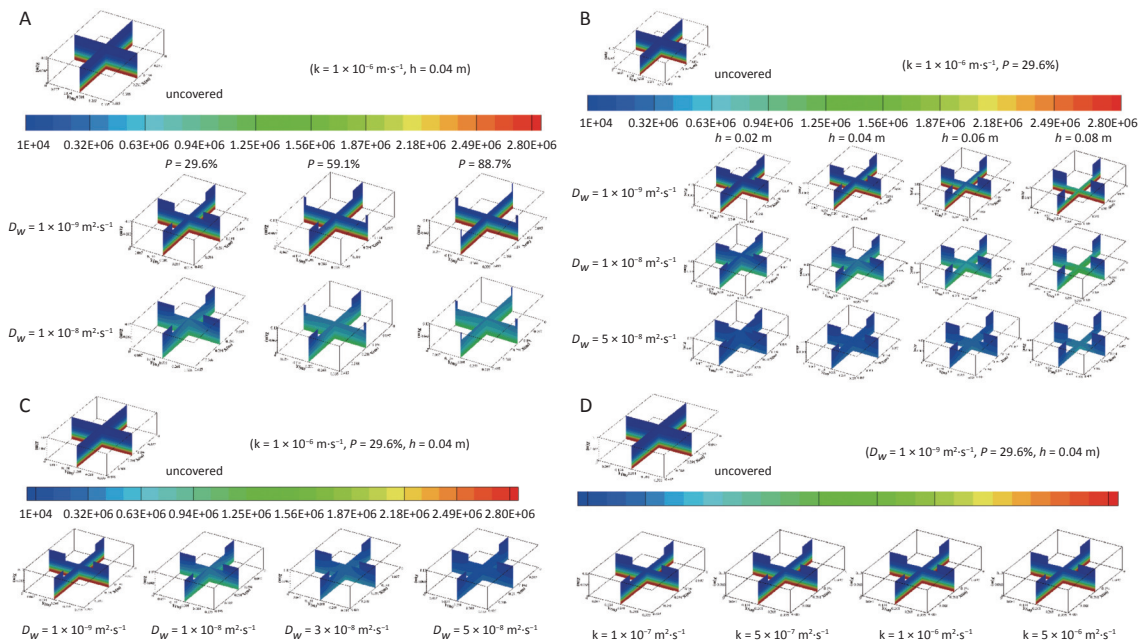

Figure 6. Radon concentration distribution in water bodies with different (A) immersion depths, (B) area coverage rates, (C) diffusion coefficients, and (D) radon transfer velocities at the gas–liquid interface. D_w, radon diffusion coefficient.

gradient in the area around the float and the radon concentration in the sediment layer decrease with an increase in the diffusion coefficient, whereas the radon concentration gradient in the sediment layer and the radon concentration in the overlying water layer first increase and then decrease.

The corresponding concentration distributions of radon for different transfer velocities at the gas–liquid interface are shown in Figure 6D. It can be observed from Figure 6D that under the same coverage conditions, the average radon concentration in the water body decreases with an increase in radon transfer velocity at the gas–liquid interface, and more radon is released to the air from the water surface.

Effect of Parameters on Radon Retardation

The calculations of the radon retardation rate with different parameters are listed in Table 1. The variations in the radon retardation rate with the area coverage rate, immersion depth diffusion coefficient, and radon transfer velocity at the gas–liquid interface are shown in Figure 7.

The variation in the radon retardation rate with the area coverage rate is shown in Figure 7A. As shown in Figure 7A, regardless of how the diffusion coefficient changes, the radon retardation rate increases with an increase in the area coverage rate, and the smaller the diffusion coefficient is, the better the radon retardation effect. Compared with those water bodies with diffusion coefficient of 1×10^{-8} $m^2 \cdot s^{-1}$, the radon retardation rates of the water bodies with diffusion coefficient of 1×10^{-9} $m^2 \cdot s^{-1}$ were increased by 28.2% and 9.8% at area coverage rate of 29.6% and 88.7%, respectively, when the immersion depth was kept the same at 0.04 m.

The variation in the radon retardation rate with the immersion depth is exhibited in Figure 7B. As shown in Figure 7B, when the thickness of the overlying water layer is small, such as 0.1 m, the radon retardation effect at different immersion depths is affected by the diffusion coefficient. For example, if the diffusion coefficient is less than 1×10^{-8} $m^2 \cdot s^{-1}$, the radon retardation rate increases first and then decreases with the increase in immersion depth. if the diffusion coefficient is greater than 5×10^{-8} $m^2 \cdot s^{-1}$, the smaller the immersion depth is, the better the radon retardation effect. For example, when the diffusion coefficient is 1×10^{-9} $m^2 \cdot s^{-1}$, the radon retardation rates increase by 1.8% when the immersion depth is increased from 0.02 to 0.06 m, and they decrease by 0.7% when the immersion depth is increased from 0.06 to 0.08 m. When the

diffusion coefficient is 1×10^{-8} $m^2 \cdot s^{-1}$, the radon retardation rates increase by 3.0% when the immersion depth is increased from 0.02 to 0.04 m and decrease by 10.8% when the immersion depth is increased from 0.04 to 0.08 m. When the diffusion coefficient is 5×10^{-8} $m^2 \cdot s^{-1}$, the radon retardation rates decrease by 34.1% when the immersion depth is increased from 0.02 to 0.08 m.

The variation in the radon retardation rate with the diffusion coefficient is shown in Figure 7C. It can be observed from Figure 7C that under the same

Table 1. Calculations of radon retardation rate

Parameters		Radon retardation rate f / %
	$P = 0$	0
	$P = 29.6\%$	28.4
$D_w = 1 \times 10^{-9}$ $m^2 \cdot s^{-1}$	$P = 59.1\%$	57.8
	$P = 88.7\%$	87.1
	$P = 0$	0
	$P = 29.6\%$	20.4
$D_w = 1 \times 10^{-8}$ $m^2 \cdot s^{-1}$	$P = 59.1\%$	47.8
	$P = 88.7\%$	78.6
	$h = 0.02$ m	28.1
	$h = 0.04$ m	28.4
$D_w = 1 \times 10^{-9}$ $m^2 \cdot s^{-1}$	$h = 0.06$ m	28.6
	$h = 0.08$ m	28.4
	$h = 0.02$ m	19.8
	$h = 0.04$ m	20.4
$D_w = 1 \times 10^{-8}$ $m^2 \cdot s^{-1}$	$h = 0.06$ m	20
	$h = 0.08$ m	18.2
	$h = 0.02$ m	11.6
	$h = 0.04$ m	11.3
$D_w = 5 \times 10^{-8}$ $m^2 \cdot s^{-1}$	$h = 0.06$ m	10.4
	$h = 0.08$ m	8.8
	$D_w = 1 \times 10^{-9}$ $m^2 \cdot s^{-1}$	28.4
	$D_w = 1 \times 10^{-8}$ $m^2 \cdot s^{-1}$	20.4
	$D_w = 3 \times 10^{-8}$ $m^2 \cdot s^{-1}$	13.9
	$D_w = 5 \times 10^{-8}$ $m^2 \cdot s^{-1}$	11.3
$P = 29.6\%$	$K = 1 \times 10^{-7}$ $m \cdot s^{-1}$	28.3
$h = 0.04$ m	$K = 5 \times 10^{-7}$ $m \cdot s^{-1}$	28.4
	$K = 1 \times 10^{-6}$ $m \cdot s^{-1}$	28.6
	$K = 5 \times 10^{-6}$ $m \cdot s^{-1}$	28.7

Note. D_w, radon diffusion coefficient; P, percentage; h, height.

covering condition, the radon retardation rate decreases with the increase in diffusion coefficient, and the decreasing rate gradually slows down. For example, when the immersion depth is 0.04 m and the area coverage rate is 29.6%, the radon retardation rates decrease by 60.2% when the diffusion coefficient is increased from 1×10^{-9} to $5 \times 10^{-8} \, \mathrm{m}^2 \cdot \mathrm{s}^{-1}$.

The variation in the radon retardation rate with the radon transfer velocity is shown in Figure 7D. As can be observed from Figure 7D, the water radon retardation rate increases with the increase in the radon transfer velocity at the gas–liquid interface, but the change is small. For example, the radon retardation rate increases by 0.01% when the radon transfer velocity is increased from 1×10^{-7} to 5×10^{-6} $\mathrm{m} \cdot \mathrm{s}^{-1}$ for a radon-containing water body under the same coverage condition.

Estimation Model of Radon Retardation Rate

The influence of the radon transfer velocity at the gas–liquid interface on radon release and the retardation effect in water bodies is minor and negligible when compared to the area-coverage rate, immersion depth, and diffusion coefficient. Based on the physical conditions and numerical simulation results of this study, the radon retardation rates of water bodies were optimally fitted for three area coverage rates (29.6%, 59.1%, 88.7%), four immersion depths (0.02, 0.04, 0.06, 0.08 m), and four diffusion coefficients (1×10^{-9}, 1×10^{-8}, 3×10^{-8}, 5×10^{-8}). The results are presented in Figure 8A, Figure 8B, and Figure 8C, along with the appropriate fitting Equation (12), Equation (13), and Equation (14).

$$f = 0.2864 - 0.058 \times h - 7776000 \times D_w - 9.521 \times 10^6 \times h \times D_w + 9.477 \times 10^{13} \times D_w^2 \, (R^2 = 0.9766)$$

(12)

$$f = 0.5813 - 0.04255 \times h - 9972000 \times D_w - 2.129 \times 10^7 \times h \times D_w + 1.111 \times 10^{14} \times D_w^2 \, (R^2 = 0.9837)$$

(13)

$$f = 0.8689 - 0.05516 \times h - 7926000 \times D_w - 3.297 \times 10^7 \times h \times D_w + 9.382 \times 10^{13} \times D_w^2 \, (R^2 = 0.9702)$$
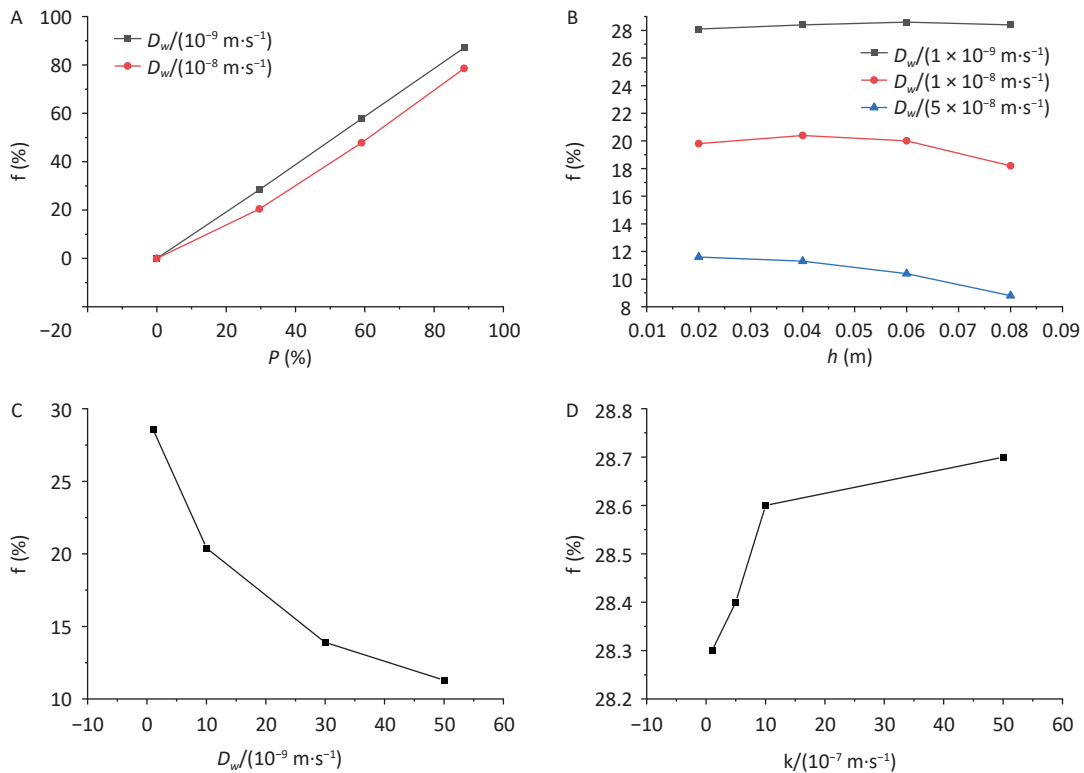
(14)

Figure 7. Variations in radon retardation rate with (A) area coverage rate, (B) immersion depth, (C) diffusion coefficient, and (D) radon transfer velocity at the gas–liquid interface. D_w, radon diffusion coefficient; P, percentage; h, height.

The estimation model for the radon retardation rate of covering floats in a water body under the synergistic effect of multiple factors (area coverage rate, immersion depth, and diffusion coefficient) was obtained as follows:

$$f = 0.01625 + 0.00943 \times P - 0.49844 \times h \\ - 4.4997 \times 10^6 \times D_w (R^2 = 0.9764) \quad (15)$$

1) From Figure 8A, Figure 8B, and Figure 8C, it can be observed that the effect of the immersion depth on the radon retardation rate is limited by the value of the diffusion coefficient under the condition of the same area coverage rate. 2) It can be observed from Equation (12), Equation (13), and Equation (14) that, when the areal coverage rate is 29.6%, the radon retardation rate can reach 28.64%; when the areal coverage rate is 59.1%, the radon retardation rate can reach 58.13%; and when the areal coverage rate is 88.7%, the radon retardation rate can reach 86.9%. 3) Equation (15) shows that, under the synergistic effect of multiple factors, the radon retardation rate is positively correlated with

Figure 8. Estimation model of radon retardation rate (A) (*P* = 29.6%), (B) (*P* = 59.1%), (C) (*P* = 88.7%).

the area coverage rate and negatively correlated with the diffusion coefficient and immersion depth.

DISCUSSION

This is a numerical simulation study of the radon retardation behavior of covering floats in radon-containing water. There has been some research on radon transportation in water[29-31], but it is new to incorporate covering methods for the same. The advantage of this study is that the distribution of radon concentrations in water can be visualized in the Figure 6, which reveals a deeper law of radon migration in water under different covering conditions. For example, with the same diffusion coefficient, the radon concentration gradient in the area around the float and in the sediment area increases with increasing immersion depth. This phenomenon can be explained as follows: a part of the radon decays before reaching the bottom of the float when the immersion depth is small, the diffusion distance of radon in the vertical direction decreases with increasing immersion depth, and more radon diffuses upward from both sides of the float and is released from the water surface before decaying. In addition, Figure 6C shows that under the same coverage conditions, the radon concentration gradient in the area around the float and the radon concentration in the sediment layer decrease with an increase in the diffusion coefficient, whereas the radon concentration gradient in the sediment and the radon concentration in the overlying water layer first increase and then decrease. This phenomenon can be explained as follows. The concentration in the overlying water layer includes the radon generated by itself and the radon transmitted by the sediment. More radon in the sediment layer is transferred to the overlying water layer. An increase in the diffusion coefficient results in a decrease in the radon concentration in the sediment layer and an increase in the radon concentration in the overlying water layer. More radon in the overlying water layer is released from the water surface with further increase in the diffusion coefficient, resulting in a gradual decrease in the radon concentration in the overlying water layer. The radon-containing water body was taken into account as a whole in the existing research on radon migration and exhalation in water[6,31]. Radon mass transport processes vary between various areas of the water and at various interfaces of the water body. We consider that not only the migration and exhalation processes of
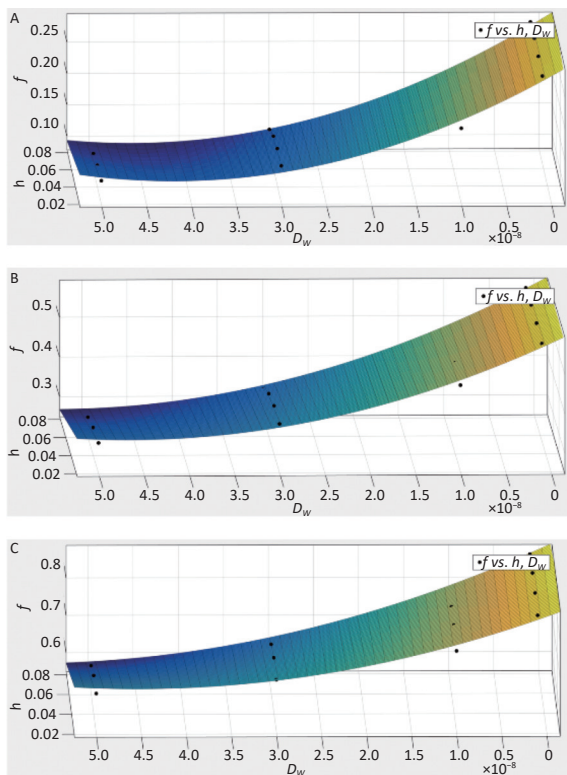
radon in the overlying water layer but also the transfer process of radon in the sediment to the overlying water layer systematically reveal the mass transfer process of radon in water under different coverage conditions.

At present, most water radon studies focus on the migration and exhalation law of water radon under the action of a single factor[32-34], and a single factor can only reveal the law under idealized conditions. In reality, water radon migration and exhalation are affected by the interaction of various factors of the exhalation law. For example, this research found that when the thickness of the overlying water layer is small, such as 0.1 m, the radon retardation effect under different immersion depths is affected by the diffusion coefficient. This phenomenon can be explained by mass conservation. According to Equation (9), the amount of radon produced by the sediment and the exposed area of the water surface remains unchanged, and the volume and amount of decayed radon of the overlying water decrease with an increase in immersion depth, resulting in an increase in radon concentration in the overlying water layer. When the diffusion coefficient is small, it is more difficult for radon from the sediment layer to migrate to the overlying water layer; therefore, the radon release rate at the water surface first decreases and then increases. However, when the diffusion coefficient is large, radon from the sediment layer is more likely to migrate to the overlying water layer, resulting in a continuous increase in the radon release rate.

Radon exhalation is affected by factors such as diffusion coefficient, free radon production rate, and radium activity concentration[32,35-36]. In recent years, covering methods have been shown to be one of the most effective methods for retarding the exhalation of radon in rocks, soil, housing building materials, and uranium tailings[14,37-38]. These studies revealed that the diffusion coefficient of the material and the mulch thickness influenced the effect of the covering method on radon exhalation. Therefore, we found that the radon retardation effect of covering floats in radon-containing water is affected by the area coverage rate, immersion depth, diffusion coefficient, and radon transfer velocity at the gas–liquid interface. We not only demonstrated the viability of this numerical simulation by experimental validation, but also studied the relationship between the radon retardation rate and these parameters. The optimized model uses multivariate linear fitting under the synergistic effects of multiple factors,

which is important for practical engineering. Fitting Eq. (15) has guiding significance for the radon prevention design of covered floats in radon-containing water; that is, under the synergistic effect of multiple factors, the area coverage rate should be increased, and the influence of some environmental factors should be minimized to reduce the diffusion coefficient. When the thickness of the overlying water layer of the sediment-containing water body is small, such as 0.1 m, the immersion depth of the float should be optimized according to the radon diffusion coefficient on the premise that the float can effectively cover the water surface. For example, if the diffusion coefficient is greater than 5×10^{-8} $m^2 \cdot s^{-1}$, the smaller the immersion depth is, the better the radon retardation effect.

CONCLUSION

To reveal the behavior of the modular floats in reducing radon release from water bodies based on the actual size of the simulated experimental device, CFD was used to simulate and compare the effects of different coverage conditions on radon retardation in radon-containing water bodies. The radon retardation rates of the simulated results were determined and the radon retardation effects were optimized and fitted. The simulated variation values of the radon retardation rate with the coverage area rates and the experimental results were compared. From the results, the following conclusions are drawn:

(1) Under the same coverage condition, the radon retardation rate of a radon-containing water body only increased by 0.01% when the radon transfer velocity at the gas–liquid interface increased from 1×10^{-7} to 5×10^{-6} $m \cdot s^{-1}$. Under the same immersion depth (0.04 m), the radon retardation rate decreased by 60.2% when the diffusion coefficient increased from 1×10^{-9} to 5×10^{-8} $m^2 \cdot s^{-1}$, whereas it increased by 2.1 times when the area coverage rate increased from 29.6% to 88.7%. When the thickness of the overlying water layer of the sediment-containing water body is small, such as 0.1 m, the immersion depth of the float should be optimized according to the radon diffusion coefficient on the premise that the float can effectively cover the water surface.

(2) Based on the physical conditions and numerical simulation results of this study, the following estimation model of the radon retardation rate of radon-containing water body coverage was

constructed using the synergistic impacts of three factors: area coverage rate, immersion depth, and diffusion coefficient: $f = 0.01625 + 0.00943 \times P - 0.49844 \times h - 4.4997 \times 10^6 \times D_w$ ($R^2 = 0.9764$). Under the synergistic effect of multiple factors, the radon retardation rate was positively correlated with the area coverage rate and negatively correlated with the diffusion coefficient and immersion depth.

(3) The numerical simulation results of the variation trend of the radon retardation rate in radon-containing water with the area coverage rate matched well with the experimental results.

AUTHOR CONTRIBUTIONS

LIU Shu Yuan: Data curation; writing–original draft; writing–review and editing; visualization. ZHANG Li: Formal analysis; Investigation; validation; review and editing. YE Yong Jun: Methodology; data curation; review and editing; funding acquisition. Ding Ku Ke: Identification of the study; review and editing of the manuscript; funding acquisition; submission of article for publication.

DECLARATION OF COMPETING INTEREST

The authors do not have any possible conflicts of interest.

REFERENCES

1. Ruano-Ravina A, Lema LV, Talavera MG, et al. Lung cancer mortality attributable to residential radon exposure in Spain and its regions. Environ Res, 2021; 199, 111372.

2. Ngoc LTN, Park D, Lee YC. Human health impacts of residential radon exposure: updated systematic review and meta-analysis of case-control studies. Int J Environ Res Public Health, 2023; 20, 97.

3. Smith H. Lung cancer risk from indoor exposure to radon daughters. Radiology, 1988; 167, 580.

4. UNSCEAR (United Nations Scientific Committee on the Effects of Atomic Radiation), Sources, effects and risks of ionizing radiation. New York: UNSCEAR. 1988.

5. Mitra S, Chowdhury S, Mukherjee J, et al. Assessment of radon (^{222}Rn) activity in groundwater and soil-gas in Purulia district, West Bengal, India. J Radioanal Nucl Chem, 2021; 330, 1331–8.

6. Carvalho FP, Oliveira JM, Lopes I, et al. Radionuclides from past uranium mining in rivers of Portugal. J Environ Radioact, 2007; 98, 298–314.

7. Groudeva VI, Groudev SN. Cleaning of acid mine drainage from an uranium mine by means of a passive treatment system. Miner Process Extr Metall Rev, 1998; 19, 89–95.

8. de Souza Pereira W, Kelecom A, Lopes JM, et al. Evaluation of the radiological quality of water released by a uranium mining in Brazil. Environ Sci Pollut Res Int, 2020; 27, 36704–17.

9. Zhang XL, Xu LC. Radiation exposure and its control measures of radon from facilities for in-situ Leaching of Uranium. Nucl Saf, 2016; 15, 17–22. (In Chinese)

10. Groudev S, Georgiev P, Spasova I, et al. Bioremediation of acid mine drainage in a uranium deposit. Hydrometallurgy, 2008; 94, 93–9.

11. Wang XX, Chen L, Wang L, et al. Synthesis of novel nanomaterials and their application in efficient removal of radionuclides. Sci China Chem, 2019; 62, 933–67.

12. Qu RX. Research on and preparation of the anti-radon coating with high performance and application test in an underground engineering. Southwest University of Science and Technology. 2012. (In Chinese)

13. Daoud WZ, Renken KJ. Laboratory assessment of flexible thin-film membranes as a passive barrier to radon gas diffusion. Sci Total Environ, 2001; 272, 127–35.

14. Deng HJ, Xiao DT, Qiu SK, et al. Reduction of radon exhalation rate through soil modified with bentonite/lime powder. Radiat Prot, 2017; 37, 280–6. (In Chinese)

15. Ye YJ, Liu SY, Xia M, et al. Experimental study on radon retardation effect of modular covering floats in radon-containing water. Environ Pollut, 2023; 331, 121915.

16. Xie D, Wang HQ, Liu ZH, et al. Numerical simulation of atmospheric dispersion of gas radioactive nuclides radon from uranium ventilation shaft exhausts. J Cent South Univ (Sci Technol), 2013; 44, 829–34. (In Chinese)

17. Rabi R, Oufni L. Study of radon dispersion in typical dwelling using CFD modeling combined with passive-active measurements. Radiat Phys Chem, 2017; 139, 40–8.

18. Rabi R, Oufni L. Evaluation of indoor radon equilibrium factor using CFD modeling and resulting annual effective dose. Radiat Phys Chem, 2018; 145, 213–21.

19. Ishimori Y, Lange K, Martin P, et al. Measurement and calculation of radon releases from NORM residues. IAEA Technical Reports Series No STI/DOC-010/474. 2013.

20. Zhang JG, Wang L, Xue YS, et al. Treatment of acidic technology effluent of one uranium mine. Uranium Min Metall, 2010; 29, 210–3. (In Chinese)

21. Ye YJ, Zhao YL, Dai XT, et al. Theoretical study on rule of radon exhalation of water-immersing particle-packing emanation media. At Energy Sci Technol, 2016; 50, 1721–8. (In Chinese)

22. Chen HL, Lian B, Yu ZX, et al. Study on the estimation method of radon exhalation rate from evaporation tank of in-situ leaching mine. Sichuan Environ, 2018; 37, 124–8. (In Chinese)

23. Wang CC, Gao X, Yao Y, et al. Investigation and analysis of environmental radioactivity for a decommissioned uranium mine in Hunan Province. Energy Res Manage, 2022(1), 99-102. (In Chinese)

24. Singh B, Singh S, Virk HS. Radon diffusion studies in air, gravel, sand, soil and water. Nucl Tracks Radiat Meas, 1993; 22, 455–8.

25. Wood WW, Kraemer TF, Shapiro A. Radon (^{222}Rn) in ground water of fractured rocks: a diffusion/ion exchange model. Ground Water, 2004; 42, 552–67.

26. Tsapalov A, Gulabyants L, Livshits M, et al. New method and installation for rapid determination of radon diffusion coefficient in various materials. J Environ Radioact, 2014; 130, 7–14.

27. Calugaru DG, Crolet JM. Identification of radon transfer velocity coefficient between liquid and gaseous phases. CR MECANIQUE, 2002; 330(5), 377-82.

28. Kawabata H, Narita H, Harada K, et al. Air-sea gas transfer velocity in stormy winter estimated from radon deficiency. J Oceanogr, 2003; 59, 651–61.

29. Cockenpot S, Claude C, Radakovitch O. Estimation of air-water

gas exchange coefficient in a shallow lagoon based on [222]Rn mass balance. J Environ Radioact, 2015; 143, 58–69.

30. Ongori JN, Lindsay R, Mvelase MJ. Radon transfer velocity at the water-air interface. Appl Radiat Isot, 2015; 105, 144–9.

31. Ye YJ, Chen GL, Dai XT, et al. Experimental study of the effect of water level and wind speed on radon exhalation of uranium tailings from heap leaching uranium mines. Environ Sci Pollut Res Int, 2019; 26, 25702–11.

32. Ye YJ, Dai XT, Ding DX, et al. Theoretical study on law of radon exhalation in radioactive water containing radon. Radiat Prot, 2017; 37, 56–61. (In Chinese)

33. Zhou J, Ding DX, Ye J. Study on the influence of temperature and humidity on radon exhalation from a radon-containing solution. J Radioanal Nucl Chem, 2018; 318, 1099–107.

34. Beg IA, Sahu P, Panigrahi DC. [222]Rn dose of mine water in different underground uranium mines. Radiat Phys Chem, 2021; 184, 109468.

35. Ye YJ, Wu WH, Feng SY, et al. Simultaneous determination of the radon diffusion coefficient and the free radon production rate from compact porous emanation media. Build Environ, 2018; 144, 66–71.

36. Hosoda M, Tokonami S, Sorimachi A, et al. Experimental system to evaluate the effective diffusion coefficient of radon. Rev Sci Instrum, 2009; 80, 013501.

37. Dong CL. Selection of tailings cover materials and determination of cover thickness for decommissioned uranium tailings impoundment. In: Seminar on Comprehensive Utilization of Tailings and Environmental Protection. 2000; 154-158. (In Chinese)

38. Deng HJ. Study on optimization of covering soil regarding reducing radon from waste dump and tailings. University of South China. 2017. (In Chinese)